INL/JOU-23-75038-Revision-0

Experimental study of mechanistic factors influencing solvent-driven fractional crystallization of calcium sulfate

February 2024

Aaron D Wilson, Liyanage Ashini Shamindra Jayasinghe, Caleb Charles Eliot Stetson, Christopher J Orme, Meng Shi

Changing the World's Energy Future

INL is a U.S. Department of Energy National Laboratory operated by Battelle Energy Alliance, LLC

INL/JOU-23-75038-Revision-0

Experimental study of mechanistic factors influencing solvent-driven fractional crystallization of calcium sulfate

Aaron D Wilson, Liyanage Ashini Shamindra Jayasinghe, Caleb Charles Eliot Stetson, Christopher J Orme, Meng Shi

February 2024

Idaho National Laboratory
Idaho Falls, Idaho 83415

http://www.inl.gov

Prepared for the
U.S. Department of Energy
Under DOE Idaho Operations Office
Contract DE-AC07-05ID14517

Experimental study of mechanistic factors influencing solvent-driven fractional crystallization of calcium sulfate

Ashini S. Jayasinghe, Caleb Stetson, Christopher J. Orme, Meng Shi, Aaron D. Wilson *

Idaho National Laboratory, PO Box 1625 MS 2208, Idaho Falls, ID 83415-2208, USA

HIGHLIGHTS

- $CaSO_4$ crystallization depends on solvent molar concentration and molecular volume.
- All solvents studied converge on a continuous pseudo-clathrate solution structure.
- Liquid DME bypasses the $CaSO_4$ crystallization induction period and increases rate.
- Reduced DME pressures are found to have advantages and disadvantages.

GRAPHICAL ABSTRACT

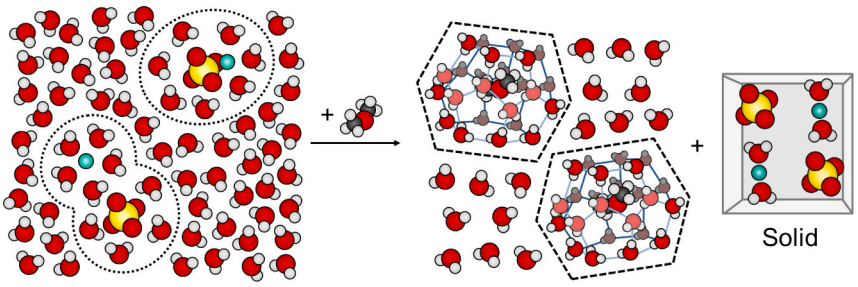

ARTICLE INFO

Keywords:
Solid-liquid equilibrium
Dimethyl ether
Softening
Hydrometallurgy
Solvent-driven fractional crystallization
Solution-based pseudo-clathrate structure

ABSTRACT

To advance dimethyl ether-driven fractional crystallization (DME-FC), a more sustainable method of water treatment and mineral recovery, a range of chemical equilibria were measured. These include varying concentrations of miscible organic solvents (MOS) used to experimentally measure the solvent-induced solid-liquid equilibrium (SLE) of calcium sulfate ($CaSO_4$) in water. Seven MOS, including dimethyl ether (DME), acetonitrile (MeCN), 1,4-dioxane, tetrahydrofuran (THF), acetone, ethanol, and diethylamine, were screened to establish trends associated with molecular volume, functional groups, and physical properties. The effect of MOS on $CaSO_4$ removal differed at concentrations <0.15 mol fraction MOS; MOS with greater molecular volume (THF, 1,4-dioxane, and diethylamine) induced greater $CaSO_4$ precipitation on a per mole basis. The solvent-induced SLE for all MOS converged between 0.15 and 0.2 mol fraction MOS, reaching a $CaSO_4$ concentration consistent with a water to MOS hydration ratio of 5:1 to 6:1, which may correspond to the solvent generating a solution-based pseudo-clathrate structure with continuity within the solution. Solution pseudo-clathrate structures provide a mechanistic basis for DME-FC.

1. Introduction

In light of surging demand for clean water, it is essential to develop a range of water purification technologies with a low carbon footprint [1,2]. Water softening [3] is an essential pretreatment for desalination as well as a standalone treatment; it is applied in residential and industrial settings (e.g., water cooling towers) when water contains too much hardness (e.g., multivalent ions) with the potential to scale water delivery systems (e.g., pipes, valves, and taps) or appliances (e.g., water heaters and tea kettles).

* Corresponding author.
E-mail address: aaron.wilson@inl.gov (A.D. Wilson).

A phenomenological relative to water treatments (including water softening) is hydrometallurgical mineral production. Hydrometallurgy has the potential to be the most cost-, energy-, and carbon-efficient method to recover many minerals from primary and recycled sources. These minerals are required for batteries [4,5], magnets [6], and alloys that underlie advanced technologies facilitating the net-carbon zero transition.

Clean, atom-efficient separations that selectively crystallize salts from solutions would benefit water softening and hydrometallurgical fractionation of mineral salts [7–11]. Membrane [12–15], electrochemical [16–18], and ion exchange [19] softening processes are prone to fouling and all produce liquid streams rich in hard ions that require disposal. Chemical softening [18,20–22], such as base softening, usually results in chemical consumption and creates waste, such as a sludge or salt added to a brine byproduct. Solvent-based aqueous treatments [23–31] isolate solids from liquids, a separation that is not generally possible with membranes, often requiring capital- and energy-intensive evaporative processes. Solvent-driven processes also avoid the chemical consumption and waste associated with chemical softening or precipitation. Specifically, solvent-driven fractional crystallization [24,26,27,32–35] selectively crystallizes salts from complex solutions with no intrinsic chemical consumption or waste production, but has historically suffered from fugitive/equilibrium losses of the solvent to the product solution and solids [23]. Selecting dimethyl ether (DME) as the crystallization agent resolves the shortcoming of solvent losses via rapid and near complete recovery of DME, as facilitated by its high vapor pressure and low enthalpy of vaporization. Advantages of dimethyl ether-driven fractional crystallization (DME-FC) include high recovery fractions (>95 %) for many salts and control of product composition with minor temperature adjustments (~10 °C) [26]. DME-FC has the potential to be a cleaner, greener, and more sustainable method to protect the environment via water softening [24], isolating valuable trace metals (waste valorization), as well as contributing to the hydrometallurgical production of minerals used in batteries and magnets [26] needed to electrify infrastructure and achieve net-zero carbon goals. However, the underlying chemical mechanisms of fractional crystallization with DME and other miscible organic solvents (MOSs) have not been supported by experimental evidence.

When a MOS is initially added to a saturated sodium chloride (NaCl) solution, a stoichiometric ratio of salt is precipitated [24,27]. Further additions of MOS to highly soluble salt solutions (based on their molar solubilities, e.g., NaCl, potassium chloride (KCl), and Magnesium Chloride ($MgCl_2$)) produce varying precipitation yields depending on the MOS. Some MOS result in diminishing stoichiometric salt removal (salt: MOS) along the SLE, while others experience a salt-induced phase separation of the MOS across a liquid-liquid equilibrium (LLE) [32–38]. In the case of moderately-to-sparingly soluble salts (based on molar solubility, e.g., $CaSO_4$, $CoSO_4$, $Sm_2(SO_4)_3$), a substantial fraction is removed (up to 98 %). However, with these high recoveries there is a stoichiometric excess of MOS relative to salt [24,26,27]. This suggests there are diminishing returns on salt precipitation as MOS concentrations are increased; however, this has not been established quantitatively.

DME-FC has potential to become a broad-spectrum softening agent, precipitating many scalants without consuming chemicals or producing additional waste, unlike other precipitation agents (bases, chemicals, and other solvents) and ion-exchange processes. The amount of DME required to treat a solution has effectively been an open question owing to a lack of experimental data and limited understanding of the precipitation mechanism. Reduced DME use would lower the system pressure and curtail the ratio of DME to treated solution, thereby reducing capital and operational costs of DME-FC. Prior to this work, the impact of varying DME pressure/concentration on the SLE of scalants has not been explored and limited experimental data [39] has shown the influence of MOS on the solubility of sparingly soluble salts like $CaSO_4$. As such, there has previously been insufficient data to ascribe a separation mechanism to organic solvent-driven precipitation of sparingly soluble salts.

This work focuses on exploring the MOS-induced SLE of sparingly soluble salts. In addition to optimizing the DME-FC softening process, this may also be useful study to probe the reduced efficacy of solvent-induced precipitation of highly soluble solutes as solvent concentration increases. The solvent-induced SLE of highly soluble salts is likely a convolution of multiple mechanisms at high MOS concentrations. In contrast, the behavior of sparingly soluble solutes may be a distinct solvent-induced SLE mechanism independent of the stoichiometric SLE mechanisms of highly soluble salts. In this work, $CaSO_4$ was selected as the salt of interest and the effects of DME, MeCN, ethanol (EtOH), 1,4-dioxane, THF, acetone, and diethylamine on the concentration of $CaSO_4$ solution were explored. Based on the results, common trends among the solvents were identified and an underlying mechanism emerged. Additionally, as DME is currently under consideration for the commercialization of solvent-driven fractional crystallization technology, the dependence of DME concentration on $CaSO_4$ precipitation rate was also studied.

2. Materials and methods

2.1. DME variable pressure precipitation of $CaSO_4$

In order to explore the impact of DME pressure on the $CaSO_4$ precipitation, a purpose-built reactor was required, as DME is in gaseous state at room temperature. A cylindrical jacketed glass reactor (Fig. 1) capped with threaded Teflon plugs at both ends was used, and DME was introduced to the reactor through a bore at the top Teflon cap. Before transferring solutions to the reactor, the system was checked for leaks using DME and purged three times with gaseous DME to remove ambient air. The saturated $CaSO_4$ solution was prepared by dissolving ACS grade $CaSO_4{\cdot}2H_2O$ in excess in 18.2 MΩ Nanopure water obtained from a PURELAB® Flex 1 system. 100 mL of saturated $CaSO_4$ solution was introduced to the reactor and liquid recirculated at a flow rate of approximately 5 mL/s using a gear pump to produce mixing. Stainless-steel mesh (316, 400 mesh, 0.0012″x48″ roll, purchased from wires

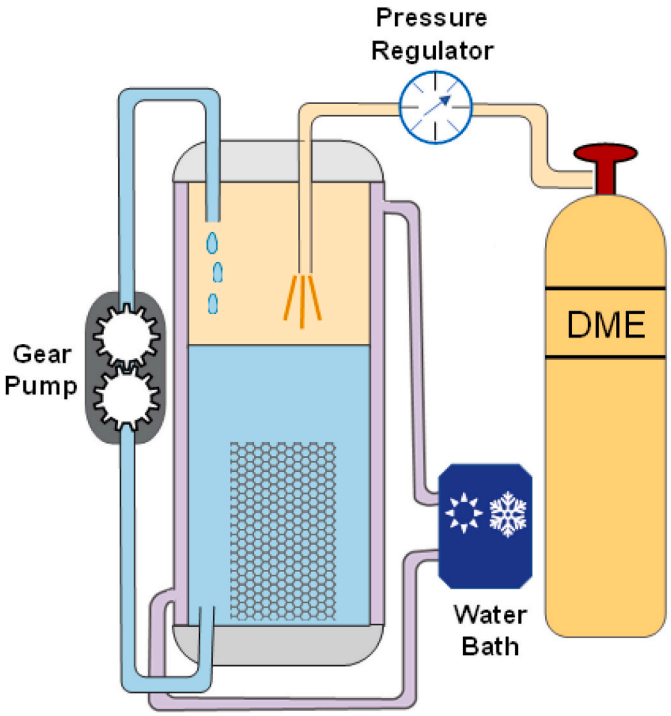

Fig. 1. Schematic representation of the reactor.

creen.org, 400x400T0012W48T) was cut to size and placed inside the reactor as a high surface area scaffold to encourage nucleation. DME was introduced as a gas of gauge-defined partial pressure (12.4 psia to 72 psia using a Swagelok® 100 psi 316 stainless-steel pressure gauge) controlled via a combination of pressure regulator and pressure relief valve in all but one experiment where liquid DME was delivered in excess at 74 psia at the initiation of the experiment. Literature data for the pressure-dependent mole fractions of DME in water at 293 K [40] were fitted to third-order polynomials. The polynomial and experimental operating pressures were used to calculate a mole fraction of DME in water for each experiment; this is displayed in Fig. SI1 in the Supporting information section.

A small but continuous DME feed was supplied to maintain a consistent pressure inside the reactor. The constant temperature of 293.15 K was maintained throughout the experiments with the assistance of a temperature-controlled water bath recirculating water through the glass jacket of the apparatus. To investigate the temporal effects on $CaSO_4$ removal, 2 mL samples were collected at different time intervals. Solutions were filtered through 0.22 μm syringe filters (Nylon, 13 mm diameter) during the sample collection to exclude solid particles from entering the sample that would subsequently experience ambient pressure (conditions under which crystallized solids would redissolve into the sample). The experiments were conducted until $CaSO_4$ concentration of the solution did not vary with time.

2.2. $CaSO_4$ precipitation with liquid MOS

Varying weight percentages of THF, MeCN, 1,4-dioxane, ethanol, acetone, and diethylamine were added to saturated $CaSO_4$ solutions. The weight percentages for the MOS ranged from 5 to 50 wt% with the total volume maintained at ~16 mL. After combining the $CaSO_4$ solutions with the MOS in a scintillation vial, the samples were left for a minimum of three days before analysis. During this time, these solutions were manually shaken at least once a day to ensure proper mixing. 5 mL aliquots from the solutions were filtered through 0.22 μm syringe filters (Nylon, 13 mm diameter) and analyzed for Ca concentration.

2.3. $CaSO_4$ concentration analysis

Ca concentration was measured using the atomic absorption spectroscopy (AAS) technique. An Agilent, 240FS AA spectrometer with a 0.5 mg/L detection limit for Ca was used for the analysis. During sample preparation for AAS, the MOS (except DME) were quenched by adding 5 μL of aqua regia to 1 mL of sample along with 3 vol% HCl used for the sample dilutions. Eliminating the organics using the aqua regia was unnecessary for the DME-treated samples, due to its high vapor pressure. The AAS measurements for each run were proportionally normalized to saturated $CaSO_4$ solution with a Ca concentration of 642 mg/L.

3. Results and discussion

3.1. Experimental precipitation of $CaSO_4$ with MOS

Solvent-induced SLE of $CaSO_4$ could be impacted by the solvent's intrinsic properties such as organic functional groups, solvent dielectric constant, and molecular volume which influence the extrinsic impact of solvent concentration. To establish the impact of these factors, this project measured the concentration of $CaSO_4$ resulting from different concentrations of seven different MOS (DME, MeCN, 1,4-dioxane, THF, acetone, ethanol, and diethylamine) to quantify their performance as fractional crystallization agents. $CaSO_4$ was selected for two reasons. Firstly, while $CaSO_4$ is a scalant and sparingly soluble, it is more soluble than many sparingly soluble materials (reaching 0.21 wt% at saturation on an anhydrous basis). Ca is an easily measured chemical species, allowing for accurate measurement of concentration of solutions depleted by solvent-driven fractional crystallization. Secondly, while lime softening (chemical precipitation via addition of calcium hydroxide, $Ca(OH)_2$ and/or related calcium bases) is a cost-effective method to remediate water hardness, treatment of sulfate-containing waters can produce treated waters that are high in $CaSO_4$. $CaSO_4$ contained in lime-softened water presents a challenge in the remediation of acid mine drainage waters, flue gas desulfurization wastewater, and other streams. Beyond these motivations, $CaSO_4$ is also expected to be representative of sparingly soluble solutes as a class. To the best of our knowledge, the only prior study of the influence of a MOS on the SLE of $CaSO_4$ is for ethanol [39]. The literature values for ethanol-H_2O-$CaSO_4$ systems were in agreement with the experimental data presented in this work (Fig. SI2).

The fraction of $CaSO_4$ removed per fraction of MOS initially added to the solution varies in seven solvent systems. At ~10 wt% (~0.03 mol fraction) solvent, the $CaSO_4$ concentration demonstrates the greatest variation ranging from 550 to 900 mg/L. At higher solvent concentrations (~40 wt%, 0.15–0.25 mol fraction), the effect of solvents on the $CaSO_4$ SLE appear to converge as all the solvents have reduced the $CaSO_4$ concentrations to <30 mg/L (see Fig. 2).

The traditional explanation for solvent-induced precipitation of salts is based on solution dielectric properties framed in a primitive implicit model of solvation. The dielectric-based rationale posits that when an organic is mixed with an aqueous brine, the result is a mixed solvent with a reduced dielectric constant that is less able to solubilize electrolytes [41–43]. Within this study 1,4-dioxane has the lowest dielectric constant and largest molecular mass (ε = 2.25 and 88.11 g/mol, respectively). If the process were driven by dielectrics, 1,4-dioxane would remove the most $CaSO_4$ per unit mass added, but this is not observed. On a mass basis, 1,4-dioxane is a less effective FC agent than the other six solvents. In fact, MeCN has the highest dielectric constant ($\varepsilon = 37.5$) and is the most effective FC agent on a mass basis (see Fig. 2a). This suggests that the salt-induced SLE mechanism is not driven by a dielectric process.

Plotting $CaSO_4$ removal against MOS mole fraction (see Fig. 2b) provides means to investigate the impact of molar properties on crystallization efficacy. 1,4-dioxane, THF, and diethylamine are the most effective in terms of mole fraction with nearly identical performance. In fact, 1,4-dioxane, THF, and diethylamine with 6, 5, and 5 heavy atoms, respectively, cleanly segregate into one cluster above a 0.05 mol fraction, while DME, ethanol, and MeCN with three heavy atoms segregate into another. Acetone with four heavy atoms falls in between these two clusters. This suggests that molecular mass and volume dictate crystallization efficacy on a molar basis. This segmentation based on molar mass/volumes when plotted against molar concentrations is further evidence of a non-primitive mole fraction-dependent mechanism (distinct from a dielectric mechanism).

The results depicted in Fig. 2 have implications to softening applications in terms of how much solvent is required to achieve a specific removal of $CaSO_4$. For example, >60 % of the $CaSO_4$ (relative to saturation) can be precipitated in the application of <25 % of the saturated concentration of DME (although more than ~50 % of the saturation pressure is required). The energy consumed by solvent-driven fractional crystallization is roughly proportional to the mass of solvent used per mass of water treated, with specific proportionality based on the individual solvent. These results indicate that a process using 9.4 wt% DME to treat a saturated solution (at ~40 psia) has a softening efficiency of 15.6 g $CaSO_4$ per Kg of DME, providing a softening efficiency ~3.5 times higher than that of a process using 37.6 wt% DME (at ~72 psia, with a softening efficiency of 3.5 g $CaSO_4$ per Kg of DME). The reduced operating pressure could also allow for less capital expenditure.

The actual increase in energy efficiency would be less for three reasons. First, natural and industrial waters are generally below saturation concentrations and the ratio of $CaSO_4$ removed per mass DME will be reduced for processes with lower initial $CaSO_4$ concentrations. For example, the tipping point when a 9.4 wt% DME process is less efficient than a 37.6 wt% DME process occurs when the initial $CaSO_4$

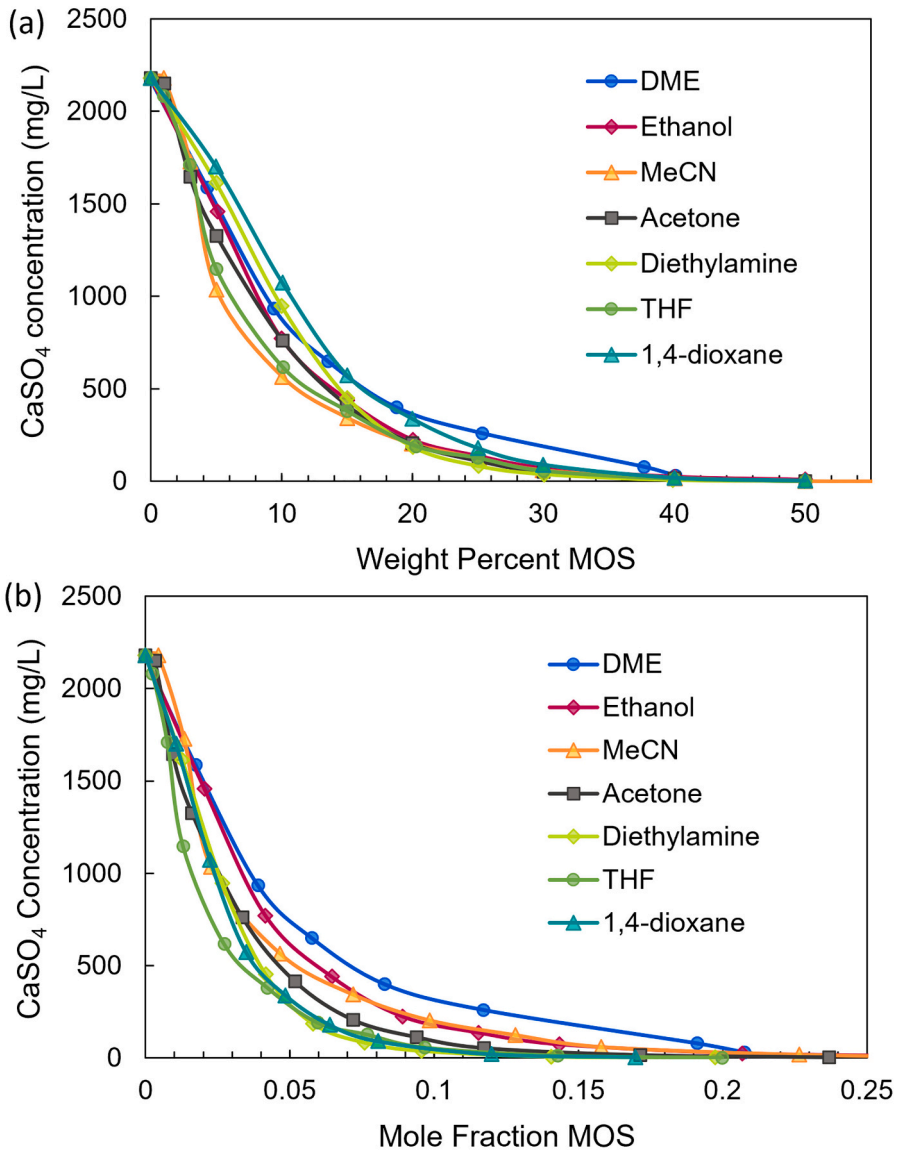

Fig. 2. SLE of $CaSO_4$ in solution versus MOS concentration plotted in terms of (a) weight percent and (b) mole fraction.

concentration drops to 51 % of its saturation concentration, where both processes achieve a softening efficiency of 1.7 g $CaSO_4$ per Kg DME. Secondly, reduced DME concentration also correlates with slower crystallization kinetics (see DME concentration-dependent $CaSO_4$ precipitation rate section) and thus requires longer residence times and higher capital costs, all other factors being equal. Lastly, while process energy (and associated capital equipment, e.g., compressors) is roughly proportional to DME concentration, the final fraction of solvent is more costly to recover (energy and capital) than the initial fractions due to mass transfer, thermodynamics (equilibrium), and other operational practicalities. For this reason, reducing DME pressure may not ultimately produce improvements to energy efficiency in softening (or hydrometallurgical processing).

These disadvantages would be less pronounced and potentially advantageous in a sequential DME-FC hydrometallurgical purification process where initial solution concentrations are saturated, DME is not fully recovered in intermediate steps, slower crystallization promotes higher purity products, and individual salt fractions can be recovered in separate stages.

3.2. *Fraction of water unavailable for $CaSO_4$ solvation*

There are multiple recent efforts to quantitatively consider solute hydration within electrolyte models; this includes work by Reynolds [44,45], Zavitas [46–49], Heyrovska [50–55], Wexler [56–60], as well as Rard and Albright [61]. Our team has developed a mass action solute speciation (MASS) model [27,62–64] in which hydration and ion-pair speciation are presumed to be governed by conventional equilibrium (i.e., mass action). The absolute concentration of highly soluble salts and MOS are modified by ion pairing and hydration to generate speciated concentrations consistent with observed water activity, i.e., vapor-liquid equilibrium (VLE) data. The hydration in this mass action model is defined by the energies of the interactions obtained from VLE data used to train the model, rather than by structure, coordination, or otherwise.

The MASS model has been successfully implemented in the modeling of VLE and predicted the solvent-induced SLE of high-activity salts (e.g., NaCl) which reach high molar concentrations and have strong interactions with a small number of waters at saturation [27,63]. However, the MASS model is not effective in predictions of $CaSO_4$, as experimentally observed $CaSO_4$ concentrations are significantly lower than predicted by MASS (Fig. 3). The MASS model trend also differs from

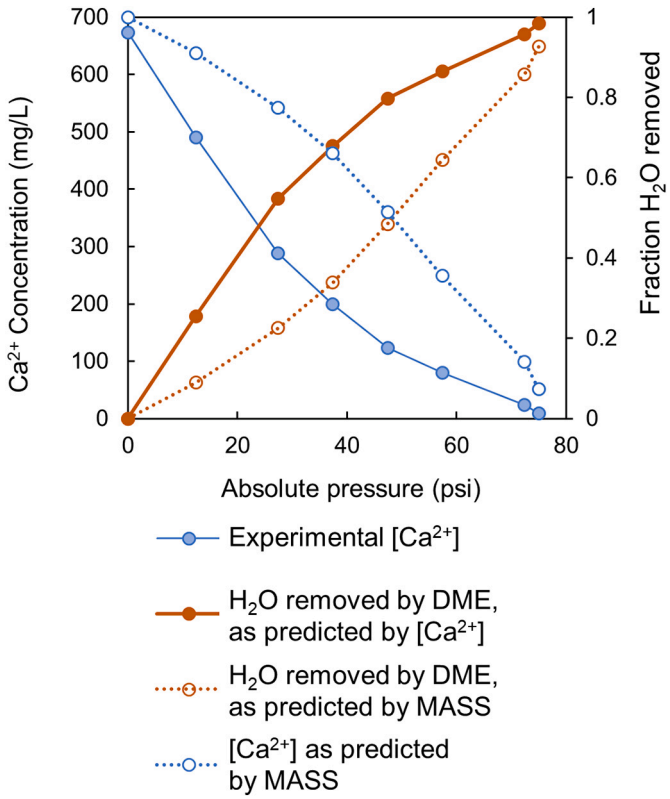

Fig. 3. Solid-liquid equilibrium (SLE) concentration of Ca^{2+} ion relative to DME vapor pressure. Fraction of hydrating water out of total water (free and hydrating) and predicted Ca^{2+} ion concentration based on mass action solution model using a DME hydration equilibrium of $K_{ha} = 6.59$.

the experimentally observed concentration-dependent trends for DME (Fig. 3).

In the MASS model, water is split into two quantities: free water and hydrating water, with the latter energetically distinct from the bulk due to strong interactions resulting from the local presence of the solute. The MASS model does not differentiate the energy states of free water, even if there is a gradient of weak interactions. Water activity is defined by the water molecule furthest from a solute, e.g., water with a marginal chemical potential (see Fig. 4). Water molecules distanced intermediately (between hydration and marginal water activity) can be expected to have energies defined by their distance from the solute. This distance-based energy well corresponds to a more concentrated solution with more extensive water structuring as water molecules approach the solute (see Fig. 4). This structuring may make intermediately distanced water unavailable in the solvation of low-activity solutes like $CaSO_4$.

Low-activity electrolytes like $CaSO_4$, which reach saturation at a low concentration, likely feature strong local interactions but also require weak interaction with long-range water to remain in solution. Low-activity solutes cannot aggressively compete for these weak interactions. A much smaller change to the chemical potential of H_2O, such as in entropically perturbed water (-0.05 kJ/mol $a_w < 0.98$ or the 55.5th water in Fig. 4), may render a solution ineffective in solvating $CaSO_4$ and result in crystallization.

Dividing the water removed, $r_{A(CaSO_4)}$, by the MOS in solution, x_{MOS}, provides an estimate of the fraction of water removed by a MOS for the purpose of $CaSO_4$ solvation at a given concentration (see Eq. (1) and Fig. 5). In Eq. (1), $[x_A]$ is water mole fraction, $[x_{CaSO_4}]$ is $CaSO_4$ concentration in solution, and $\left[x^*_{CaSO_4}\right]$ is saturated $CaSO_4$ concentration.

$$r_{A(CaSO_4)} = 1 - \frac{[x_{CaSO_4}] \Big/ \left[x^*_{CaSO_4}\right]}{[x_A]} \tag{1}$$

At low concentrations, all MOS except THF approach $r_{A(CaSO_4)}$ values of 15:1 to 25:1, corresponding to cages found in Type I and II clathrates of 20:1 to 28:1 [65,66]. THF approaches a $r_{A(CaSO_4)}$ value of 36:1 at low concentrations, corresponding to a water molecule to cavity ratio of 36:1 in a single large Type H clathrate. These values converge at higher concentrations (0.15–0.20 mol fraction), specifically converging to a $r_{A(CaSO_4)}$ ratio of 5:1 to 6:1, which is the ratio of water molecules to cavities in a continuous Type I and II clathrate. These data provide evidence of solution-state pseudo-clathrate structures [67–70]. While solution-state pseudo-clathrate structures have been observed spectroscopically and have attracted theoretical interest, this report is the first indication of clathrate formation resulting in a convergent structure for a variety of MOS.

A continuous, solution-based clathrate structure may provide a structural description of microstructure that is common in binary water-organic mixtures, especially MeCN [71–73]. The complexity in the transition between Henry's law solute behavior and microstructural domain may be an organization of discrete individual clathrate cages into a supramolecular continuous structure common to solid clathrates.

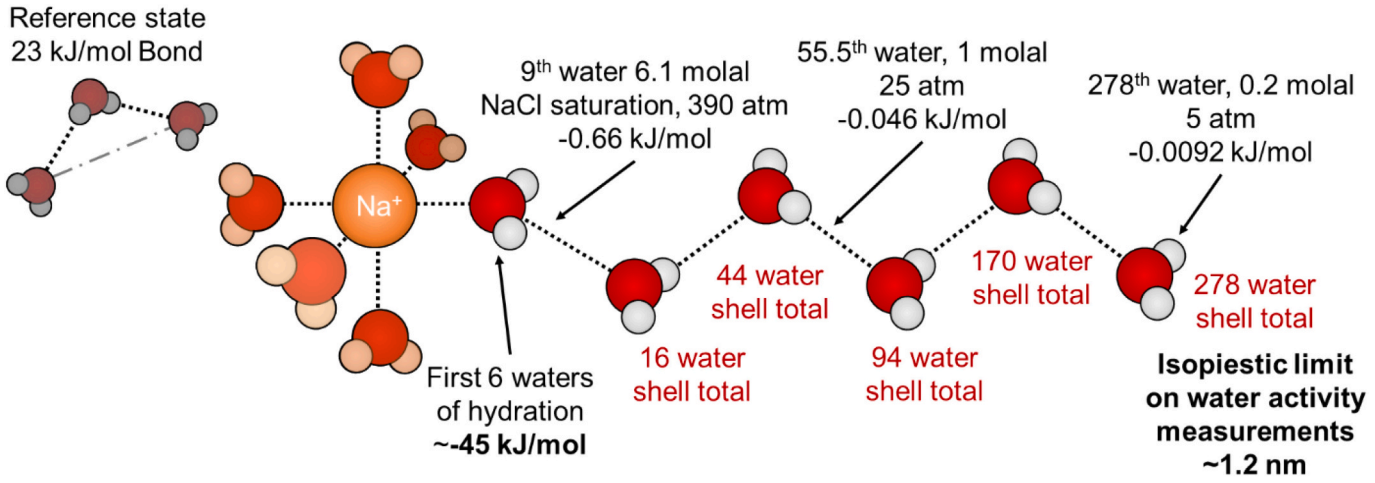

Fig. 4. The chemical potential of water (i.e., VLE and water activity)-defined distance from a solute and its relationship to concentration in high-activity NaCl salt solution according to MASS.

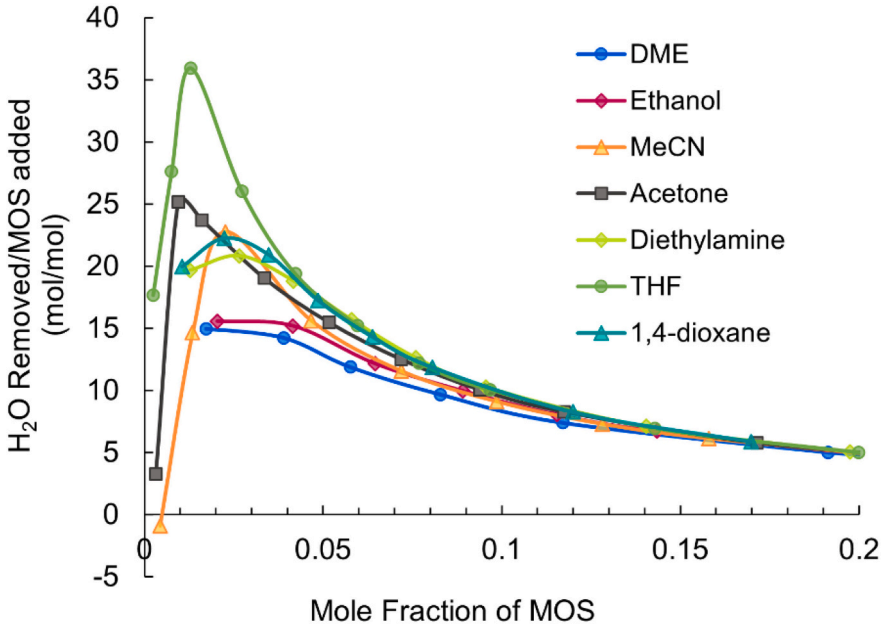

Fig. 5. H_2O removed per MOS added was plotted vs. mole fraction MOS based on $CaSO_4$ removal via Eq. (1).

3.3. DME concentration-dependent $CaSO_4$ precipitation rate

DME-FC of $CaSO_4$ is also a temporal process (Fig. 6a). While the experimental apparatus was designed to encourage crystallization (inclusion of a high surface area scaffold and likelihood of suspended nanocrystals originating from the saturated $CaSO_4$ solution), it is limited to observing crystallization trends and cannot separate contributions of mass transfer kinetics. Despite these limits, it was noted throughout the experiments that the solution appeared homogenous based on visual observations of the liquid, including suspended solids, suggesting good mixing and limited impact of macroscopic localization of the solution. To ensure these systems have reached equilibrium, the experiments were carried out until the $CaSO_4$ concentration was constant with time. While the x-axis in Fig. 6 includes data for 500 min, data was collected for 840 and 720 min at 12.4 and 72.4 psi, respectively. When gaseous DME is delivered, the experimental apparatus has an induction period in the precipitation of $CaSO_4$ on the order of 60 min (at 72.4 psi) to 150 min (at 27.4 psi). It must be noted that Ostwald ripening processes affect measurement of the induction period, in the instance that coarsening of $CaSO_4$ particles has not proceeded to the extent that crystalline solids are captured by the filter (0.2 μm). Broadly, the induction period likely occurs due to a combination of factors; these may include i) limited mass transport rates for DME vapor diffusing into the aqueous phase (a VLE phenomenon), ii) crystallization kinetics that change based on the concentration of DME within the system (an SLE phenomenon), and iii) the contribution from the existence of a separate liquid DME phase to the coarsening and growth of solids in the reactor environment (LLE and SLE phenomena). Lastly, the system was optimized for operability (e.g., avoiding the formation of gas-liquid dispersion or foam) rather than mass transfer of DME into the aqueous system; thus, it is likely that mass transfer could be further improved. After this induction period, there are one or more kinetic domains prior to approaching equilibrium $CaSO_4$ concentrations. When liquid DME is delivered to the system, the induction period is eliminated (see Fig. 6b).

Maintaining and recirculating liquid DME in the precipitation vessel of an industrial system will enhance the application of DME-FC in softening. Based on the experimental data for $CaSO_4$ crystallization with liquefied DME, a residence time of 20 min or less would result in effective softening; however, recirculatory $CaSO_4$ seeding and enhanced mixing could further reduce this time in an industrial process.

4. Conclusion

The degree of $CaSO_4$ precipitation suggests that as MOS is added to a solution, the water is structured around the MOS, rendering a portion of the water unavailable for $CaSO_4$ solvation. $CaSO_4$ appears to be sensitive to low-energy water structuring. Initial $CaSO_4$ removal by MOS varies with the MOS's molecular volume on a molar concentration basis, with larger MOS occupying more water. With further addition of MOS, the ratio of water removed to MOS added becomes consistent with a continuous solution of type I or II clathrate structures. Upon completion of the pseudo-clathrate structure, no more functional water is available to solubilize $CaSO_4$ and 98–99 % of the low-activity salt is crystallized from solution. The impact of reducing DME pressure/concentration on softening and hydrometallurgical processes has advantages (improved $CaSO_4$ to DME precipitation ratio depending on initial $CaSO_4$ concentration and reduced operational pressure) and disadvantages (an induction period, greater sensitivity to the initial $CaSO_4$ concentration, reduced $CaSO_4$ precipitation kinetics, and more costly DME recovery per mass DME). Introducing a molecular volume-based structuring of water as a mechanistic basis for $CaSO_4$ precipitations with organic solvents provides a path to interpret the precipitation of other minerals in water treatment and hydrometallurgical purifications via DME-FC.

CRediT authorship contribution statement

Ashini S. Jayasinghe: Writing – review & editing, Visualization, Investigation. **Caleb Stetson:** Writing – review & editing, Visualization, Investigation. **Christopher J. Orme:** Methodology. **Meng Shi:** Writing – review & editing, Investigation. **Aaron D. Wilson:** Writing – original draft, Visualization, Supervision, Project administration, Methodology, Funding acquisition, Conceptualization.

Declaration of competing interest

The authors declare the following financial interests/personal relationships which may be considered as potential competing interests: Aaron D Wilson reports financial support was provided by the Solar Energy Technology Office via the DOE American-Made Solar Desalination Prize. Aaron D Wilson, Caleb Stetson, Christopher Orme has patent #US 11,261,111 issued to Assignee Battelle Energy Alliance LLC. Aaron

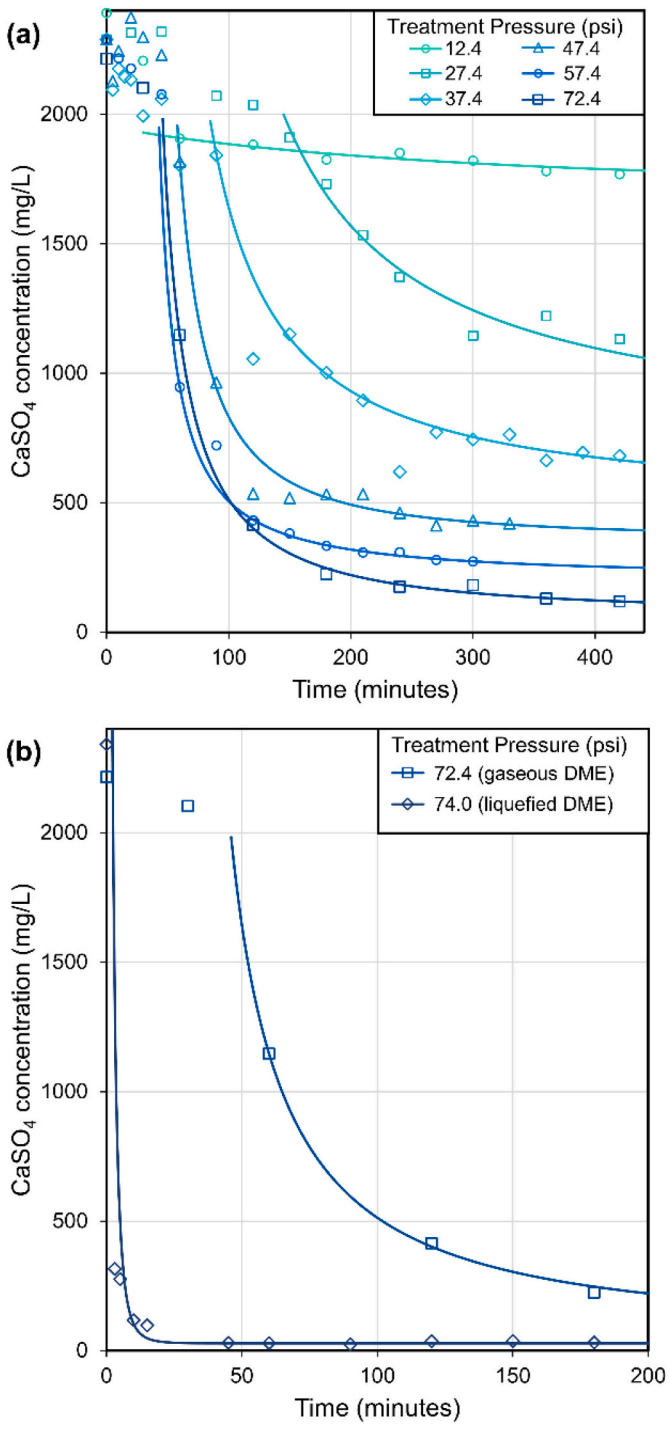

Fig. 6. (a) Ca concentration versus time at varied gaseous DME pressures. (b) Ca concentration versus time comparing gaseous and liquefied DME delivery.

D Wilson, Caleb Stetson, Christopher Orme has patent #PCT/US2022/072792 pending to Assignee Battelle Energy Alliance LLC. If there are other authors, they declare that they have no known competing financial interests or personal relationships that could have appeared to influence the work reported in this paper.

Acknowledgements

This work was supported by the United States Department of Energy at Idaho National Laboratory through contract DE-AC07-05ID14517. Funding was supplied by the Solar Energy Technology Office via the DOE American-Made Solar Desalination Prize. We thank John Webley and Nehemiah Ceasar of Trevi Systems and the rest of The Hard Ion Team (HIT) for support and input during the development of this work.

Appendix A. Supplementary data

Supplementary data to this article can be found online at https://doi.org/10.1016/j.desal.2024.117474.

References

[1] J. Strutt, S. Wilson, H. Shorney-Darby, A. Shaw, A. Byers, Assessing the carbon footprint of water production, J. AWWA 100 (2008) 80–91, https://doi.org/10.1002/j.1551-8833.2008.tb09654.x.
[2] M. Li, L. Duan, S. Li, H. Zhang, Q. Gao, S.W. Hermanowicz, Carbon emission calculations and reductions in membrane water treatment: a review, ACS EST Water. 4 (2024) 20–32, https://doi.org/10.1021/acsestwater.3c00559.
[3] C. Tang, M. Rygaard, P.S. Rosshaug, J.B. Kristensen, H.-J. Albrechtsen, Evaluation and comparison of centralized drinking water softening technologies: effects on water quality indicators, Water Res. 203 (2021) 117439, https://doi.org/10.1016/j.watres.2021.117439.
[4] D.J. Garole, R. Hossain, V.J. Garole, V. Sahajwalla, J. Nerkar, D.P. Dubal, Recycle, recover and repurpose strategy of spent Li-ion batteries and catalysts: current status and future opportunities, ChemSusChem 13 (2020) 3079–3100, https://doi.org/10.1002/cssc.201903213.
[5] H. Bastos, N. Schaeffer, J.M. Pringle, J.A.P. Coutinho, C. Pozo-Gonzalo, Enhanced dissolution of metal oxides in hydroxylated solvents – towards application in lithium-ion battery leaching, ChemSusChem 16 (2023) e202300455, https://doi.org/10.1002/cssc.202300455.
[6] X. Xu, S. Sturm, Z. Samardzija, J. Vidmar, J. Scancar, K.Z. Rozman, Direct recycling of Nd–Fe–B magnets based on the recovery of Nd2Fe14B grains by acid-free electrochemical etching, ChemSusChem 12 (2019) 4754–4758, https://doi.org/10.1002/cssc.201902342.
[7] S.E. Can Sener, V.M. Thomas, D.E. Hogan, R.M. Maier, M. Carbajales-Dale, M. D. Barton, T. Karanfil, J.C. Crittenden, G.L. Amy, Recovery of critical metals from aqueous sources, ACS Sustainable, Chem. Eng. 9 (2021) 11616–11634, https://doi.org/10.1021/acssuschemeng.1c03005.
[8] A. Kumar, G. Naidu, H. Fukuda, F. Du, S. Vigneswaran, E. Drioli, J.H.V. Lienhard, Metals recovery from seawater desalination brines: technologies, opportunities, and challenges, ACS Sustain. Chem. Eng. 9 (2021) 7704–7712, https://doi.org/10.1021/acssuschemeng.1c00785.
[9] H. Jin, D.M. Park, M. Gupta, A.W. Brewer, L. Ho, S.L. Singer, W.L. Bourcier, S. Woods, D.W. Reed, L.N. Lammers, J.W. Sutherland, Y. Jiao, Techno-economic assessment for integrating biosorption into rare earth recovery process, ACS Sustain. Chem. Eng. 5 (2017) 10148–10155, https://doi.org/10.1021/acssuschemeng.7b02147.
[10] B.A. Sharkh, A.A. Al-Amoudi, M. Farooque, C.M. Fellows, S. Ihm, S. Lee, S. Li, N. Voutchkov, Seawater desalination concentrate—a new frontier for sustainable mining of valuable minerals, Npj Clean Water. 5 (2022) 1–16, https://doi.org/10.1038/s41545-022-00153-6.
[11] J.J. Lado, R.L. Zornitta, I. Vázquez Rodríguez, K. Malverdi Barcelos, L.A. M. Ruotolo, Sugarcane biowaste-derived biochars as capacitive deionization electrodes for brackish water desalination and water-softening applications, ACS Sustainable, Chem. Eng. 7 (2019) 18992–19004, https://doi.org/10.1021/acssuschemeng.9b04504.
[12] M. Bodzek, S. Koter, K. Wesołowska, Application of membrane techniques in a water softening process, Desalination 145 (2002) 321–327, https://doi.org/10.1016/S0011-9164(02)00430-7.
[13] B. Su, T. Wu, Z. Li, X. Cong, X. Gao, C. Gao, Pilot study of seawater nanofiltration softening technology based on integrated membrane system, Desalination 368 (2015) 193–201, https://doi.org/10.1016/j.desal.2015.03.012.
[14] O. Labban, T.H. Chong, J.H. Lienhard, Design and modeling of novel low-pressure nanofiltration hollow fiber modules for water softening and desalination pretreatment, Desalination 439 (2018) 58–72, https://doi.org/10.1016/j.desal.2018.04.002.
[15] Y. Xu, Q.-B. Chen, J. Wang, P.-F. Li, J. Zhao, Fractionation of monovalent ions from seawater brine via softening nanofiltration and selective electrodialysis: which is better? Desalination 533 (2022) 115717 https://doi.org/10.1016/j.desal.2022.115717.
[16] C. Gabrielli, G. Maurin, H. Francy-Chausson, P. Thery, T.T.M. Tran, M. Tlili, Electrochemical water softening: principle and application, Desalination 201 (2006) 150–163, https://doi.org/10.1016/j.desal.2006.02.012.
[17] J. Choi, P. Dorji, H.K. Shon, S. Hong, Applications of capacitive deionization: desalination, softening, selective removal, and energy efficiency, Desalination 449 (2019) 118–130, https://doi.org/10.1016/j.desal.2018.10.013.
[18] X. Ba, J. Chen, X. Wang, H. Xu, J. Sun, Y. Qi, Y. Li, J. Wang, B. Jiang, An integrated electrolysis-microfiltration-ion exchange closed-loop system for effective water softening without chemicals input and spent regenerant discharge, Desalination 553 (2023) 116481, https://doi.org/10.1016/j.desal.2023.116481.
[19] A. Venkatesan, P.C. Wankat, Simulation of ion exchange water softening pretreatment for reverse osmosis desalination of brackish water, Desalination 271 (2011) 122–131, https://doi.org/10.1016/j.desal.2010.12.022.

[20] Y. Zhao, H. Cao, Y. Xie, J. Yuan, Z. Ji, Z. Yan, Mechanism studies of a CO2 participant softening pretreatment process for seawater desalination, Desalination 393 (2016) 166–173, https://doi.org/10.1016/j.desal.2015.12.014.

[21] O. Kedem, G. Zalmon, Compact accelerated precipitation softening (CAPS) as a pretreatment for membrane desalination I, Softening by NaOH, Desalination. 113 (1997) 65–71, https://doi.org/10.1016/S0011-9164(97)00115-X.

[22] A. Masarwa, D. Meyerstein, N. Daltrophe, O. Kedem, Compact accelerated precipitation softening (CAPS) as pretreatment for membrane desalination II, Lime softening with concomitant removal of silica and heavy metals, Desalination. 113 (1997) 73–84, https://doi.org/10.1016/S0011-9164(97)00116-1.

[23] Z.H. Foo, C. Stetson, E. Dach, A. Deshmukh, H. Lee, A.K. Menon, R. Prasher, N. Y. Yip, J.H. Lienhard, A.D. Wilson, Solvent-driven aqueous separations for hypersaline brine concentration and resource recovery, Trends in Chemistry. 4 (2022) 1078–1093, https://doi.org/10.1016/j.trechm.2022.09.004.

[24] J.S. McNally, Z.H. Foo, A. Deshmukh, C.J. Orme, J.H. Lienhard, A.D. Wilson, Solute displacement in the aqueous phase of water–NaCl–organic ternary mixtures relevant to solvent-driven water treatment, RSC Adv. 10 (2020) 29516–29527, https://doi.org/10.1039/D0RA06361D.

[25] A. Deshmukh, Z.H. Foo, C. Stetson, H. Lee, C.J. Orme, A.D. Wilson, J.H. Lienhard, Thermodynamics of solvent-driven water extraction from hypersaline brines using dimethyl ether, Chem. Eng. J. 434 (2022) 134391, https://doi.org/10.1016/j.cej.2021.134391.

[26] C. Stetson, D. Prodius, H. Lee, C. Orme, B. White, H. Rollins, D. Ginosar, I. C. Nlebedim, A.D. Wilson, Solvent-driven fractional crystallization for atom-efficient separation of metal salts from permanent magnet leachates, Nat. Commun. 13 (2022) 3789, https://doi.org/10.1038/s41467-022-31499-7.

[27] A.D. Wilson, Z.H. Foo, A.S. Jayasinghe, C. Stetson, H. Lee, H.W. Rollins, A. Deshmukh, J.H. Lienhard, Modeling Henry's law and phase separations of water–NaCl–organic mixtures with solvation and ion-pairing, Phys. Chem. Chem. Phys. (2023), https://doi.org/10.1039/D3CP02003G.

[28] C. Boo, R.K. Winton, K.M. Conway, N.Y. Yip, Membrane-less and non-evaporative desalination of hypersaline brines by temperature swing solvent extraction, Environ. Sci. Technol. Lett. 6 (2019) 359–364, https://doi.org/10.1021/acs.estlett.9b00182.

[29] C. Boo, I.H. Billinge, X. Chen, K.M. Shah, N.Y. Yip, Zero liquid discharge of ultrahigh-salinity brines with temperature swing solvent extraction, Environ. Sci. Technol. 54 (2020) 9124–9131, https://doi.org/10.1021/acs.est.0c02555.

[30] R.T. Berry, E. Dach, J.A. Melhorn, N.Y. Yip, L. Soh, Assessing the Temperature-dependent tunable polarity of N,N-Dimethylcyclohexylamine (DMCHA) and water mixtures, ACS Sustain. Chem. Eng. 10 (2022) 3726–3734, https://doi.org/10.1021/acssuschemeng.2c00293.

[31] K.M. Shah, I.H. Billinge, E. Dach, N.Y. Yip, Advancing the productivity-selectivity trade-off of temperature swing solvent extraction desalination with intermediate-step release, Environ. Sci. Technol. Lett. 10 (2023) 949–954, https://doi.org/10.1021/acs.estlett.3c00616.

[32] Z.B. Alfassi, The separation of electrolytes in aqueous solution by miscible organic solvents, Sep. Sci. Technol. 14 (1979) 155–161, https://doi.org/10.1080/01496397908062552.

[33] Z.B. Alfassi, L. Ata, Separation of the system NaCl-NaBr-NaI by "solventing out" from aqueous solution, Sep. Sci. Technol. 18 (1983) 593–601, https://doi.org/10.1080/01496398308060298.

[34] Z.B. Alfassi, S. Mosseri, Solventing out of electrolytes from their aqueous solution, AICHE J. 30 (1984) 874–876, https://doi.org/10.1002/aic.690300539.

[35] S. Mosseri, Z.B. Alfassi, The measurement of the solubility of electrolytes in water—miscible organic solvent mixture by using the "solventing out" process, Chem. Eng. Sci. 40 (1985) 1695–1701, https://doi.org/10.1016/0009-2509(85)80030-0.

[36] Z.B. Alfassi, L. Feldman, The preparation of carrier free radiobromine: the separation of KBrO3 and KBr using an organic solvent, Int. J. Appl. Radiat. Isot. 27 (1976) 125–126, https://doi.org/10.1016/0020-708X(76)90188-5.

[37] S. Mosseri, Z.B. Alfassi, Separation of the KX-KXO3-KXO4 (X = Cl, Br, I) system by "solventing-out" processes, Sep. Sci. Technol. 18 (1983) 165–175, https://doi.org/10.1080/01496398308055666.

[38] Z.B. Alfassi, The separation of electrolytes by a "solventing-out" process, AICHE J. 31 (1985) 506–507, https://doi.org/10.1002/aic.690310325.

[39] V. Gomis, M.D. Saquete, J. García-Cano, CaSO4 solubility in water–ethanol mixtures in the presence of sodium chloride at 25°C, Application to a reverse osmosis process, Fluid Phase Equilibria. 360 (2013) 248–252, https://doi.org/10.1016/j.fluid.2013.09.063.

[40] H. Holldorff, H. Knapp, Binary vapor-liquid-liquid equilibrium of dimethyl ether - water and mutual solubilities of methyl chloride and water: experimental results and data reduction, Fluid Phase Equilib. 44 (1988) 195–209, https://doi.org/10.1016/0378-3812(88)80111-0.

[41] R. Govind, R. Foster, Systems, apparatus, and methods for separating salts from water, US20140158616A1. https://patents.google.com/patent/US20140158616A1/en?oq=US20140158616A1, 2014. (Accessed 17 October 2018).

[42] Y. Ma, M. Svärd, X. Xiao, J.M. Gardner, R.T. Olsson, K. Forsberg, Precipitation and crystallization used in the production of metal salts for Li-ion battery materials: a review, Metals 10 (2020) 1609, https://doi.org/10.3390/met10121609.

[43] Y. Wada, M. Matsumoto, K. Onoe, Antisolvent crystallization of NaCl using the minute-bubble technique – effects of different antisolvent types, J. Cryst. Growth 448 (2016) 76–81, https://doi.org/10.1016/j.jcrysgro.2016.03.043.

[44] J.G. Reynolds, A method to apply Zavitsas' aqueous electrolyte model to multicomponent solutions and its equivalence to Zdanovskii's rule, AICHE J. 68 (2022) e17487, https://doi.org/10.1002/aic.17487.

[45] J.G. Reynolds, T.R. Graham, C.I. Pearce, Extending Zavitsas' hydration model to the thermodynamics of solute mixtures in water, J. Mol. Liq. 347 (2022) 118309, https://doi.org/10.1016/j.molliq.2021.118309.

[46] A.A. Zavitsas, Properties of water solutions of electrolytes and nonelectrolytes, J. Phys. Chem. B 105 (2001) 7805–7817, https://doi.org/10.1021/jp011053l.

[47] A.A. Zavitsas, The nature of aqueous solutions: insights into multiple facets of chemistry and biochemistry from freezing-point depressions, Chemistry – A, European Journal. 16 (2010) 5942–5960, https://doi.org/10.1002/chem.200903063.

[48] A.A. Zavitsas, Quest to demystify water: ideal solution behaviors are obtained by adhering to the equilibrium mass action law, J. Phys. Chem. B 123 (2019) 869–883, https://doi.org/10.1021/acs.jpcb.8b07166.

[49] A.A. Zavitsas, Ideal thermodynamic behaviors of aqueous electrolyte solutions at very high concentrations, Chem. Phys. Lett. 759 (2020) 137941, https://doi.org/10.1016/j.cplett.2020.137941.

[50] R. Heyrovska, A reappraisal of Arrhenius' theory of partial dissociation of electrolytes, in: Electrochemistry, Past and Present, American Chemical Society, 1989, pp. 75–91, https://doi.org/10.1021/bk-1989-0390.ch006.

[51] R. Heyrovská, Degrees of dissociation and hydration numbers of alkali halides in aqueous solutions at 25 °C (some up to saturation), Croat. Chem. Acta 70 (1997) 39–54.

[52] R. Heyrovská, Volumes of ions, ion pairs, and electrostriction of alkali halides in aqueous solutions at 25°C, Mar. Chem. 70 (2000) 49–59, https://doi.org/10.1016/S0304-4203(00)00014-1.

[53] R. Heyrovska, Degrees of dissociation and hydration numbers of M2SO4 (M= H, Li, Na, K, Rb, Cs and NH4) in aq. solns at 25 C, Electroanalysis 18 (2006) 351–361.

[54] R. Heyrovská, Ionic concentrations and hydration numbers of "supporting electrolytes, Electroanalysis 18 (2006) 351–361, https://doi.org/10.1002/elan.200503416.

[55] R. Heyrovska, Partial dissociation and hydration quantitatively explain the properties of aqueous electrolyte solutions and hence empirical activity concepts are unnecessary, Nature Precedings 1 (2011), https://doi.org/10.1038/npre.2011.6416.1.

[56] A.S. Wexler, Raoult was right after all, ACS Omega 4 (2019) 12848–12852, https://doi.org/10.1021/acsomega.9b01707.

[57] A.S. Wexler, K. Patel, M. Gen, C.K. Chan, Reconciling measurement and prediction of free and solvated water in solution, ACS Omega. 5 (2020) 8754–8765, https://doi.org/10.1021/acsomega.0c00311.

[58] A.S. Wexler, Raoult was right after all: statistical mechanics derivation and volumetric validation, Fluid Phase Equilib. 531 (2021) 112899, https://doi.org/10.1016/j.fluid.2020.112899.

[59] A.S. Wexler, A step-wise ion hydration model of aqueous electrolyte solution: the 1:1 punch, Fluid Phase Equilib. (2022) 113498, https://doi.org/10.1016/j.fluid.2022.113498.

[60] M. Arrad, A.S. Wexler, A step-wise ion hydration model of aqueous electrolyte solution: the 2:2, 2:1 and 1:2 punches, Fluid Phase Equilib. 566 (2023) 113694, https://doi.org/10.1016/j.fluid.2022.113694.

[61] J.A. Rard, J.G. Albright, Expressions for the activity coefficients and osmotic coefficients of solutions of electrolytes and nonelectrolytes based on the hydration model of Zavitsas, J. Solut. Chem. 43 (2014) 172–185, https://doi.org/10.1007/s10953-013-0121-8.

[62] A.D. Wilson, H. Lee, C. Stetson, Local stress within a granular molecular solvent matrix, a mechanism for individual ion hydration, J. Mol. Liq. 361 (2022) 119544, https://doi.org/10.1016/j.molliq.2022.119544.

[63] A.D. Wilson, H. Lee, C. Stetson, Mass action model of solution activity via speciation by solvation and ion pairing equilibria, Commun Chem. 4 (163) (2021) 1–8, https://doi.org/10.1038/s42004-021-00599-8.

[64] A.D. Wilson, C. Stetson, Modeling solution vapor equilibria with solvation and solute assembly, J. Mol. Liq. 336 (2021) 116272, https://doi.org/10.1016/j.molliq.2021.116272.

[65] T. Miyoshi, M. Imai, R. Ohmura, K. Yasuoka, Thermodynamic stability of type-I and type-II clathrate hydrates depending on the chemical species of the guest substances, J. Chem. Phys. 126 (2007) 234506, https://doi.org/10.1063/1.2746324.

[66] E.D. S.J., A. Koh Carolyn, Clathrate Hydrates of Natural Gases, 3rd ed, CRC Press, Boca Raton, 2007, https://doi.org/10.1201/9781420008494.

[67] T. Head-Gordon, Is water structure around hydrophobic groups clathrate-like? Proc. Natl. Acad. Sci. 92 (1995) 8308–8312, https://doi.org/10.1073/pnas.92.18.8308.

[68] W.-H. Hsu, T.-C. Yen, C.-C. Chen, C.-W. Yang, C.-K. Fang, I.-S. Hwang, Observation of mesoscopic clathrate structures in ethanol-water mixtures, J. Mol. Liq. 366 (2022) 120299, https://doi.org/10.1016/j.molliq.2022.120299.

[69] R. Li, C. D'Agostino, J. McGregor, M.D. Mantle, J.A. Zeitler, L.F. Gladden, Mesoscopic structuring and dynamics of alcohol/water solutions probed by terahertz time-domain spectroscopy and pulsed field gradient nuclear magnetic resonance, J. Phys. Chem. B 118 (2014) 10156–10166, https://doi.org/10.1021/jp502799x.

[70] T.A. Dolenko, S.A. Burikov, S.A. Dolenko, A.O. Efitorov, I.V. Plastinin, V. I. Yuzhakov, S.V. Patsaeva, Raman spectroscopy of water–ethanol solutions: the estimation of hydrogen bonding energy and the appearance of clathrate-like structures in solutions, J. Phys. Chem. A 119 (2015) 10806–10815, https://doi.org/10.1021/acs.jpca.5b06678.

[71] R. Macchieraldo, S. Gehrke, N.K. Batchu, B. Kirchner, K. Binnemans, Tuning solvent miscibility: a fundamental assessment on the example of induced

methanol/n-dodecane phase separation, J. Phys. Chem. B 123 (2019) 4400–4407, https://doi.org/10.1021/acs.jpcb.9b00839.
[72] S. Koley, S. Ghosh, A deeper insight into an intriguing acetonitrile–water binary mixture: synergistic effect, dynamic Stokes shift, fluorescence correlation spectroscopy, and NMR studies, Phys. Chem. Chem. Phys. 18 (2016) 32308–32318, https://doi.org/10.1039/C6CP05024G.
[73] J.J. Shephard, S.K. Callear, S. Imberti, J.S.O. Evans, C.G. Salzmann, Microstructures of negative and positive azeotropes, Phys. Chem. Chem. Phys. 18 (2016) 19227–19235, https://doi.org/10.1039/C6CP02450E.